Sliding mode-based lateral vehicle dynamics control using tyre force measurements

Anil Kunnappillil Madhusudhanan[a]*, Matteo Corno[a,b] and Edward Holweg[a,c]

[a]*Intelligent Automotive Systems Group, Precision and Microsystems Engineering Department, Delft University of Technology, Mekelweg 2, 2628 CD Delft, The Netherlands;* [b]*Dipartimento di Elettronica, Informazione e Bioingegneria, Politecnico di Milano, Via Ponzio 34/5, 20133 Milano, Italy;* [c]*SKF Automotive Division, Kelvinbaan 16, 3430 DT Nieuwegein, The Netherlands*

(*Received 18 July 2014; accepted 17 June 2015*)

1. Introduction

Vehicle dynamics controllers (VDC) are used to improve vehicle performance and safety. They keep the vehicle stable when a driver pushes the vehicle towards its unstable region of operation. An average skilled driver might do so as parameters such as tyre–road friction and vehicle load are prone to change depending on different driving conditions. VDCs can be broadly classified into longitudinal, lateral and vertical dynamics control systems. In this work, only lateral VDC (LVDC) is considered.

There are several ways to design LVDCs. Many of the existing systems are based on yaw rate measurement. Vehicle yaw rate is compared with a reference and a corrective control is applied using braking or steering actuators.[1–3] Another LVDC approach is to act up on the error between estimated vehicle side slip angle and its reference.[4] However, yaw rate $\dot{\psi}$ and vehicle side slip angle β dynamics are dependent on tyre forces, and undesired yaw rate or vehicle side slip angle is a result of undesired tyre forces. In [1], a linear tyre model is used and this can cause the control action to be not optimal when the tyres are in the nonlinear operating region. In [2], the nonlinear tyre model from Pacejka [5] is used to

*Corresponding author. Email: a.k.madhu@tudelft.nl

address this issue. However, the nonlinear tyre model from Pacejka is prone to change as the friction characteristic changes. Then, the tyre force calculations may not be correct and therefore control action using yaw rate or vehicle side slip angle may not be optimal. Hence, controlling tyre forces instead of yaw rate or vehicle side slip angle could bring considerable benefits in stability and performance.

At the same time, accurate estimation of tyre force is a challenging task; in the past few years, several approaches have been developed.[6,7] In [6], an indirect method based on accelerometers fixed inside the tyres is proposed. Whereas in [7], a more direct method based on load sensing bearing is proposed. The progress in the technology in the past few years has made it possible to have usable prototypes. In this work, we will refer to the load sensing bearing technology developed by SKF and installed in our test vehicle.

In [8–10], the tyre force-based approach is successfully applied to longitudinal vehicle dynamics control. In [11], the lateral vehicle stability is improved by equalising the tyre utilisation coefficients (TUCs). TUC is an indication of how much the tyre is engaged with respect to the maximum force it can exert. The basic principle is to equalise the left and right TUC of the front axle using active independent front steering. By doing so, saturation during cornering can be avoided or delayed, thereby improving stability. Although steer-by-wire is not yet an off-the-shelf technology, active steering is being researched very actively. This warrants the study and design of VDC systems based on active steering.

In this work, the LVDC proposed in [11] is extended in several directions.

- The nonlinearities and uncertainties of the vehicle model are considered. In order to address them, an output tracking sliding-mode control (SMC) is designed and validated. The final SMC is gain scheduled with respect to vehicle velocity.
- An active steering system model is considered to incorporate steering actuator dynamics.
- The effect of the proposed controller on vehicle lateral acceleration is studied. On a typical dry road, lateral tyre force has a peak value corresponding to a certain tyre side slip angle. This implies that, if a driver applies more steering assuming he will get more lateral acceleration and stability is not lost in the process, he might in fact be settling for a lower lateral acceleration. With the proposed controller, a vehicle can maintain the maximum possible lateral tyre forces and therefore maintain the maximum possible lateral acceleration for higher steering angles.
- The SMC is studied for its robustness against vehicle velocity, force measurement noise and road–tyre friction.

This paper is structured as follows. Section 2 shows the vehicle model used to design the controller. In Section 3, the controller design is explained in detail. The controller is simulated in closed loop and the results are discussed in Section 4. Section 5 concludes the findings and discusses possible future work.

2. Lateral vehicle dynamics modelling

A four-wheeled vehicle equipped with independent front steering and tyre force sensors is assumed. The car is equipped with two front wheel load sensing bearing hubs measuring the tyre longitudinal, lateral and vertical forces. In the following, two models of a four-wheeled vehicle are employed. The vehicle model used for simulation is a multi-body model with 15 mechanical degrees of freedom from CarSim simulation package.[12] The CarSim model uses a nonlinear tyre model with dependency on slip, load and camber. A standard hatchback vehicle is simulated (see the vehicle configuration *Ind_Ind: B-Class, Hatchback: No ABS* in

CarSim for more details about the vehicle model). The considered vehicle has the following parameters.

- Mass: 1231 kg.
- Yaw inertia: 2031.4 kgm^2.
- Distance from centre of gravity (CoG) to front axle: 1.016 m.
- Distance from CoG to rear axle: 1.562 m.
- Distance between left and right tyres: 1.539 m.

For the controller design, a control-oriented double track model as shown in Figure 1 with states yaw rate $\dot{\psi}$ and vehicle side slip angle β is used. The model outputs are front left lateral tyre force $F_{y_{\mathrm{FL}}}$ and front right lateral tyre force $F_{y_{\mathrm{FR}}}$. The control inputs are front left road steering angle δ_{FL} and front right road steering angle δ_{FR}. The simplified state equations are shown in Equations (1) and (2).

$$\dot{\beta} = \frac{1}{Mv}(F_{y_{\mathrm{FL}}} + F_{x_{\mathrm{FL}}}\delta_{\mathrm{FL}} + F_{y_{\mathrm{FR}}} + F_{x_{\mathrm{FR}}}\delta_{\mathrm{FR}} + F_{y_{\mathrm{RL}}} + F_{y_{\mathrm{RR}}}) - \frac{\beta}{Mv}(F_{x_{\mathrm{FL}}} - F_{y_{\mathrm{FL}}}\delta_{\mathrm{FL}} + F_{x_{\mathrm{FR}}} - F_{y_{\mathrm{FR}}}\delta_{\mathrm{FR}} + F_{x_{\mathrm{RL}}} + F_{x_{\mathrm{RR}}} - c_{\mathrm{aer}}A_L\frac{\rho}{2}v^2) - \dot{\psi}, \tag{1}$$

$$J_z\ddot{\psi} = (F_{y_{\mathrm{FR}}} + F_{x_{\mathrm{FR}}}\delta_{\mathrm{FR}} + F_{y_{\mathrm{FL}}} + F_{x_{\mathrm{FL}}}\delta_{\mathrm{FL}})a - (F_{y_{\mathrm{RL}}} + F_{y_{\mathrm{RR}}})b + (F_{x_{\mathrm{RR}}} - F_{x_{\mathrm{RL}}})s + (F_{x_{\mathrm{FR}}} - F_{y_{\mathrm{FR}}}\delta_{\mathrm{FR}})s - (F_{x_{\mathrm{FL}}} - F_{y_{\mathrm{FL}}}\delta_{\mathrm{FL}})s. \tag{2}$$

Here M is the vehicle mass, v is the velocity, $F_{y_{ij}}$ is the lateral tyre force of ij tyre, $F_{x_{ij}}$ is the longitudinal tyre force of ij tyre, δ_{ij} is the road steering angle, c_{aer} is the coefficient of aerodynamic drag, A_L is the front vehicle area, ρ is the air density and J_z is the moment of inertia around yaw axis. a, b and s are vehicle dimensions as shown in Figure 1. It is assumed that the steering angles are small so that $\cos\delta_{ij} \approx 1$ and $\sin\delta_{ij} \approx \delta_{ij}$. The output equations are shown in Equations (3) and (4).

$$F_{y_{\mathrm{FL}}} = C_{y_{\mathrm{FL}}}\left(\delta_{\mathrm{FL}} - \left(\beta + \frac{\dot{\psi}a}{v}\right)\right), \tag{3}$$

$$F_{y_{\mathrm{FR}}} = C_{y_{\mathrm{FR}}}\left(\delta_{\mathrm{FR}} - \left(\beta + \frac{\dot{\psi}a}{v}\right)\right). \tag{4}$$

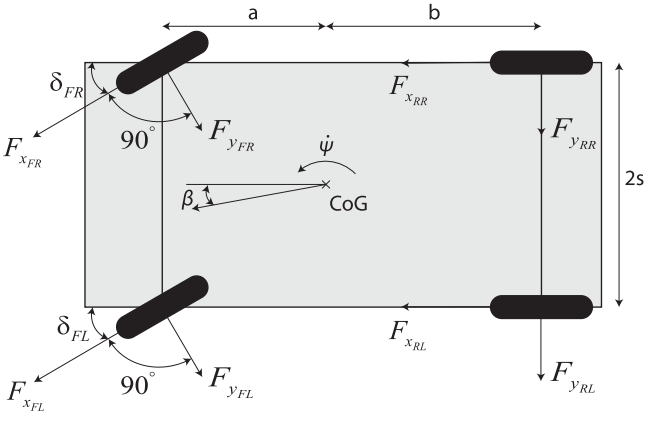

Figure 1. Simplified vehicle model used for controller design.

Here $C_{y_{ij}}$ is the cornering stiffness of the ij tyre. They are calculated from the linear region of the CarSim tyre model. Further, the state and output equations in Equations (1)– (4) are lin-earised with $v = 80$ km/h and no steering wheel angle as shown in Equations (5) and (6). The model parameters for linearisation are obtained from the CarSim vehicle model and a CarSim simulation performed at $v = 80$ km/h while driving straight. The linearisation vehicle speed is chosen as 80 km/h as the controller is first studied with $v = 80$ km/h.

The linearised model inevitably introduces some approximations and uncertainties. In order to account for them, it is assumed that the model uncertainties and nonlinearities lie in the image of input matrix B_i and feedthrough matrix D_i as shown in Equations (5) and (6). This assumption, which is required for the SMC design, is called matching condition.[13]

$$\dot{\tilde{x}} = A_i\tilde{x} + B_iu + B_ie_x(t), \tag{5}$$

$$y = C_i\tilde{x} + D_iu + D_ie_y(t). \tag{6}$$

Here $\tilde{x} = \{\beta, \dot{\psi}\}$, $u = \{\delta_{\mathrm{FL}}, \delta_{\mathrm{FR}}\}$ and $y = \{F_{y_{\mathrm{FL}}}, F_{y_{\mathrm{FR}}}\}$. A_i, B_i, C_i and D_i are linearised system matrices. $e_x(t)$ and $e_y(t)$ are vectors that lump all the model uncertainties and nonlinearities in the state and output equations, respectively.

Since the objective is lateral tyre forces tracking, the system state vector is augmented with the integral of the lateral force tracking errors,

$$x_{a_{\mathrm{FL}}} = \int (F^{\mathrm{ref}}_{y_{\mathrm{FL}}} - F_{y_{\mathrm{FL}}})\,\mathrm{d}t, \tag{7}$$

$$x_{a_{\mathrm{FR}}} = \int (F^{\mathrm{ref}}_{y_{\mathrm{FR}}} - F_{y_{\mathrm{FR}}})\,\mathrm{d}t, \tag{8}$$

$$\dot{x} = \begin{bmatrix} A_i & 0 \\ -C_i & 0 \end{bmatrix} x + \begin{bmatrix} B_i \\ -D_i \end{bmatrix} u + \begin{bmatrix} B_i & 0 \\ 0 & -D_i \end{bmatrix} e + \begin{bmatrix} 0 \\ I \end{bmatrix} r. \tag{9}$$

Here $x = \{\beta, \dot{\psi}, x_{a_{\mathrm{FL}}}, x_{a_{\mathrm{FR}}}\}$, $e = \{e_x(t), e_y(t)\}$ and r is the reference lateral tyre force vector $\{F^{\mathrm{ref}}_{y_{\mathrm{FL}}}, F^{\mathrm{ref}}_{y_{\mathrm{FR}}}\}$. Using $A = \left[\begin{smallmatrix} A_i & 0 \\ -C_i & 0 \end{smallmatrix}\right]$, $B_1 = \left[\begin{smallmatrix} B_i \\ -D_i \end{smallmatrix}\right]$, $B_e = \left[\begin{smallmatrix} B_i & 0 \\ 0 & -D_i \end{smallmatrix}\right]$ and $B_2 = \left[\begin{smallmatrix} 0 \\ I \end{smallmatrix}\right]$ gives

$$\dot{x} = Ax + B_1u + B_ee + B_2r. \tag{10}$$

2.1. *Steering actuator control*

The vehicle is assumed to have an active steering system for the front wheels.[14,15] The overall steering actuator control (SAC), accounting for the dynamics of the actuator and bandwidth of the steering control system, is assumed to have a closed-loop bandwidth of 10 Hz.

Two of such SACs, SAC left (SACL) and SAC right (SACR), are used, one for the front left wheel and the other for the front right wheel. The SACs are considered to be a part of the vehicle as the lateral dynamics controller applies control input to the SACs. In the next section, the lateral dynamics controller is discussed.

3. Lateral dynamics control

In this section, the lateral dynamics control structure and its design is explained. The con-trol structure is shown in Figure 2. The controller, named tyre utilisation coefficient control (TUCC), generates the desired road steering angles for the front left and front right tyres

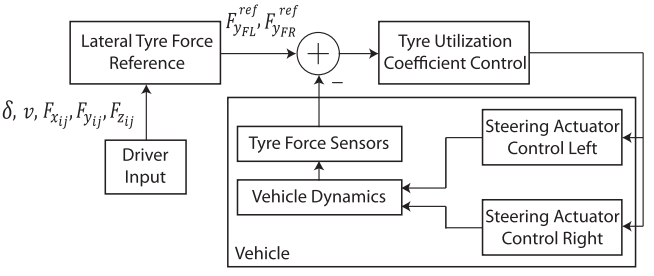

Figure 2. Control scheme of the proposed TUCC.

and are applied to the SAC left and right (SACL and SACR). TUCC is a nonlinear control based on the sliding mode and is designed considering the vehicle model uncertainties and nonlinearities.

3.1. *Tyre utilisation coefficient control*

The TUCC is designed with the objective of keeping the vehicle stable in the lateral direction; this is achieved by forcing the lateral tyre forces to track a computed reference value. The reference lateral tyre forces are generated such that both the front left and front right tyres have equal TUC.

3.1.1. *Tyre utilisation coefficient*

TUC k is defined in Equation (11) and is shown graphically using the friction ellipse in Figure 3. It is an indication of how much the tyre is engaged with respect to the maximum force it can exert.

$$k = \frac{F_x^2}{F_{x_{\max}}^2} + \frac{F_y^2}{F_{y_{\max}}^2} \quad \text{where } 0 <= k <= 1. \tag{11}$$

Here F_x is the longitudinal tyre force, F_y is the lateral tyre force, $F_{x_{\max}}$ is the maximum possible longitudinal tyre force and $F_{y_{\max}}$ is the maximum possible lateral tyre force. F_x and F_y are highly nonlinear functions of slip ratio, side slip angle, camber and vertical load. $F_{x_{\max}}$ and $F_{y_{\max}}$ depend on many factors; among them are peak road–tyre friction and vertical forces. The vertical force measurement is available from the force sensors. There are several works

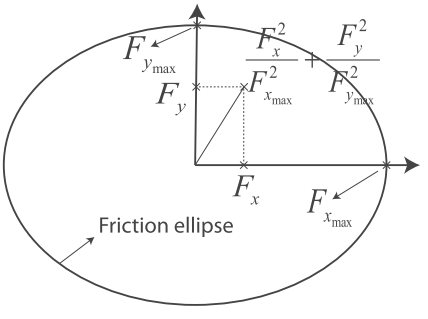

Figure 3. Definition of tyre utilisation coefficient k using friction ellipse.

published on peak road–tyre friction estimation. As the focus of this work is lateral dynamics control, the peak road–tyre friction is assumed to be available using one of the estimation methods from the literature.[16–19]

TUCs are zero when the vehicle is still on a horizontal surface or when the tyres are freely rolling. They are one when the tyres are exerting the maximum possible force in longitudinal, lateral or an intermediate direction. In different driving conditions, the vehicle tyres might employ different TUCs. For instance, during a steady-state cornering, because of lateral acceleration, if the vehicle CoG is above the roll centre, lateral load transfer will load the outer tyres more than the inner tyres. This can cause unequal TUCs between the outer and inner tyres because of the nonlinear characteristics of tyre dynamics, steering system and suspension camber.

To understand this better, the behaviour of the TUCs is studied for various lateral accelerations during steady-state cornering. Figure 4 shows the TUCs of the front left tyre k_{FL} and the front right tyre k_{FR} for various lateral accelerations a_y. The tyre side slip angles of the front left tyre α_{FL} and the front right tyre α_{FR} are also shown. In this set of simulations, the left tyre is the inner tyre and the radius of curvature (RoC) is 100 m.

From Figure 4, it is observed that the inner TUC, k_{FL}, is always higher than the outer TUC, k_{FR}. This is caused by the geometry and compliances of the steering and suspension systems. As a consequence, the inner wheel reaches higher tyre side slip (see Figure 4). This means that the natural lateral tyre forces do not yield equal TUCs. Hence, all tyres would not have equal reserve, and this might lead to the saturation of TUC of one of the tyres when another tyre is under employed. This might cause an average skilled driver to loose control. The rear TUCs k_{RL} and k_{RR} also have the same behaviour; however, the difference is much less than the front tyres.

If the vehicle can be controlled so that equal right and left TUCs are obtained, the saturation of the inner TUC can be avoided or delayed, thereby assisting the driver in keeping the vehicle stable.

Another interesting driving situation to study TUCs is a constant speed cornering where an average skilled driver applies steering higher than a certain threshold. On a typical dry road, the lateral tyre force has a peak value corresponding to a certain tyre side slip angle. Its effect is shown in Figure 5 where the steering wheel angle is increased till 300° at a constant vehicle speed of 80 km/h. It can be observed that the lateral acceleration reaches its peak around 135° steering wheel angle and then the lateral acceleration decreases. This means that the driver is settling for an undesired lower lateral acceleration value. In terms of TUCs, it means that, instead of the front tyre TUCs being one, they might be lower than one as shown

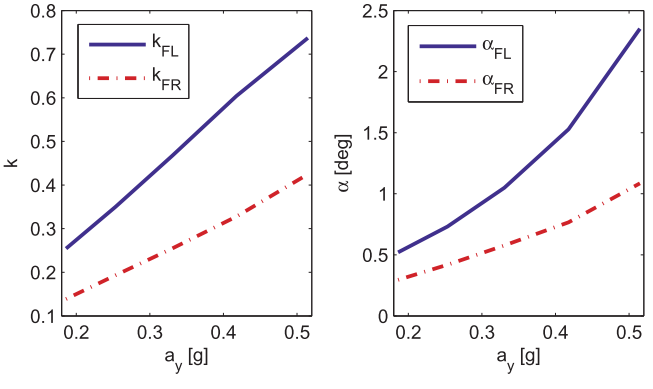

Figure 4. TUC study during steady-state cornering manoeuvres.

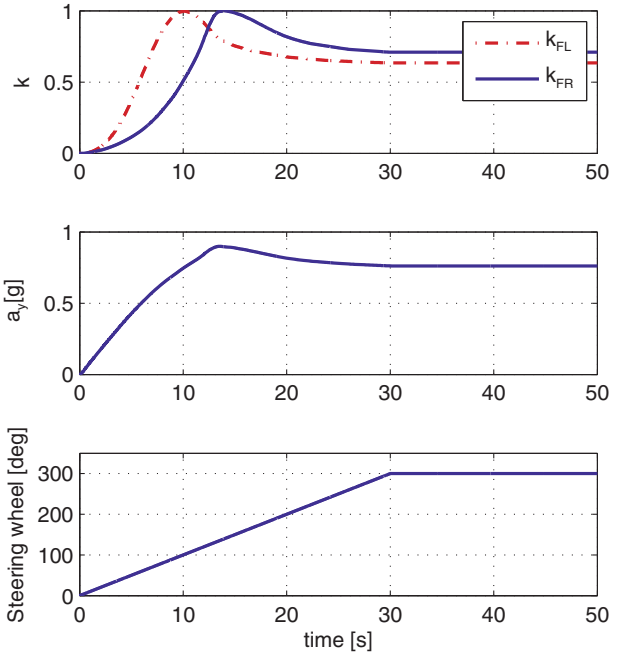

Figure 5. Effect of driver steering wheel on lateral acceleration on a dry road.

in the top plot of Figure 5. Thereby, the lateral acceleration reduces as the steering wheel value is increased from 135°, which is undesirable.

With the proposed controller, a vehicle can maintain the maximum possible lateral tyre forces and therefore maintain the maximum possible lateral acceleration for higher steering angles.

In the next section, the points discussed are further studied with the help of a closed-loop controller.

3.1.2. *TUCC design*

The TUCC structure is shown in Figure 2. The schematic has two main components: a lateral force controller tuned to track a reference and a lateral force reference generator. The *Lateral tyre force reference* generator computes the reference according to two objectives. The first objective is to guarantee that the front right and left TUCs are equal; the second objective is to force a desired dynamics on the vehicle. As a result of the desired dynamics defined by the second objective, the vehicle can maintain the maximum possible lateral acceleration for higher steering angles. The first objective is given in Equation (12).

$$k_{\mathrm{FL}} = k_{\mathrm{FR}} = k_F^{\mathrm{req}}, \tag{12}$$

$$k_{ij} = \frac{F_{x_{ij}}^2}{F_{x_{ij\max}}^2} + \frac{F_{y_{ij}}^2}{F_{y_{ij\max}}^2}. \tag{13}$$

Here k_F^{req} is the required TUC of the front axle tyres. Further, the lateral tyre force reference values considering a desired vehicle dynamics are calculated using the reference generator in Figure 2.

The driver's steering input δ, vehicle velocity v, and force sensor measurements $\{F_{x_{ij}}, F_{y_{ij}}, F_{z_{ij}}\}$ are given as inputs to the reference generator. The desired dynamics is expressed through the understeering gradient according to

$$R_{\text{req}} = \frac{1}{\delta}\left(a + b + \frac{v^2\eta}{g}\right), \tag{14}$$

$$a_y^{\text{req}} = \frac{v^2}{R_{\text{req}}} \quad \text{with limits } \{-\mu_y g, \mu_y g\}, \tag{15}$$

$$k_F^{\text{req}} = \frac{|a_y^{\text{req}}|}{\mu_y g} + \frac{F_{x_{Fq}}^2}{F_{x_{Fq\max}}^2} \quad \text{with limits } \{0, 1\}. \tag{16}$$

Here, R_{req} is the RoC of the curve the vehicle is trying to negotiate, η is the desired understeer coefficient and a_y^{req} is the lateral acceleration required in order to negotiate the curve with RoC R_{req}. The value of η is chosen as 0.0171 rad/g, the understeer coefficient of the linearised CarSim vehicle model. a_y^{req} has saturation limits based on the considered road friction μ_y and gravity g. $F_{x_{Fq}}^2/F_{x_{Fq\max}}^2$ in Equation (16) is defined as follows.

$$\frac{F_{x_{Fq}}^2}{F_{x_{Fq\max}}^2} = \begin{cases} \dfrac{F_{x_{\text{FL}}}^2}{F_{x_{FL\max}}^2} & \text{if } \dfrac{F_{x_{\text{FL}}}^2}{F_{x_{FL\max}}^2} \geq \dfrac{F_{x_{\text{FR}}}^2}{F_{x_{\text{FR}\max}}^2}, \\ \dfrac{F_{x_{\text{FR}}}^2}{F_{x_{\text{FR}\max}}^2} & \text{otherwise.} \end{cases} \tag{17}$$

The second controller objective is given in Equation (16) and as a result of this objective, when the driver applies higher steering angle such that $|v^2/R_{\text{req}}| > \mu_y g$, k_F^{req} will be 1. This would cause the vehicle to maintain the maximum possible lateral acceleration which depends on the longitudinal tyre forces. Finally, the lateral tyre force reference values are calculated depending on the longitudinal tyre forces ,[1]

$$F_{y_{\text{FL}}}^{\text{ref}} = \sqrt{\left(k_F^{\text{req}} - \frac{F_{x_{\text{FL}}}^2}{F_{x_{FL\max}}^2}\right)} F_{y_{FL\max}} \operatorname{sign}(F_{y_{\text{FL}}}), \tag{18}$$

$$F_{y_{\text{FR}}}^{\text{ref}} = \sqrt{\left(k_F^{\text{req}} - \frac{F_{x_{\text{FR}}}^2}{F_{x_{\text{FR}\max}}^2}\right)} F_{y_{\text{FR}\max}} \operatorname{sign}(F_{y_{\text{FR}}}). \tag{19}$$

The maximum possible tyre forces $F_{x_{ij\max}}$ and $F_{y_{ij\max}}$ are calculated based on the vertical tyre force $F_{z_{ij}}$ and the peak road–tyre friction. Here $\operatorname{sign}(F_{y_{ij}})$ is 1 if $F_{y_{ij}} >= 0$ and -1 otherwise. $F_{y_{\text{FL}}}^{\text{ref}}$ and $F_{y_{\text{FR}}}^{\text{ref}}$ are calculated in Equations (18) and (19) such that the TUCC objectives $k_{\text{FL}} = k_{\text{FR}} = k_F^{\text{req}}$ in Equation (12) and $k_F^{\text{req}} = |a_y^{\text{req}}|/\mu_y g + F_{x_{Fq}}^2/F_{x_{Fq\max}}^2$ with limits $\{0, 1\}$ in Equation (16) are met.

Based on the lateral force references in Equations (18) and (19), and the vehicle model in Equation (10), the TUCC is designed. Considering sensor noise, vehicle model nonlinearities and vehicle model uncertainties, SMC is chosen in virtue of its robustness characteristic (see [13,20] for more details on SMC).

Controller: The SMC is defined by Equations (20)–(22). As seen in Equation (20), the control has two parts, a continuous and a discontinuous one. u_{eq} is the continuous part and is the equivalent control assuming the lumped vector e in Equation (10) to be zero. u_N is the

discontinuous part that compensates the uncertainties and nonlinearities.

$$u = u_{\text{eq}} + u_N \quad \text{where} \tag{20}$$

$$u_{\text{eq}} = -(C_s B_1)^{-1} C_s (Ax + B_2 r), \tag{21}$$

$$u_N = -\frac{B_1^{\text{T}} C_s^{\text{T}} C_s x}{\|B_1^{\text{T}} C_s^{\text{T}} C_s x\|_2} \gamma. \tag{22}$$

Here $\gamma = \rho + \alpha$ where $\rho > \|(B_i^{\text{T}} B_i + D_i^{\text{T}} D_i)^{-1} [B_i^{\text{T}} B_i \;\; D_i^{\text{T}} D_i] e\|_2$ (B_i and D_i are the input and feedthrough matrices from Equations (5) and (6)) and α is a positive number.

Proposition: Given the controller (20)–(22) and the model defined in Equation (10), the sliding surface in Equation (24) is attractive for the closed-loop system.

$$S = \begin{bmatrix} 0 & 0 & 1 & 0 \\ 0 & 0 & 0 & 1 \end{bmatrix}, \quad x = 0, \tag{23}$$

$$= C_s x = 0. \tag{24}$$

Physical interpretation of the above equation is that when the vehicle states x satisfy Equation (24), the lateral tyre forces $\{F_{y_{\text{FL}}}, F_{y_{\text{FR}}}\}$ track their reference $\{F_{y_{\text{FL}}}^{\text{ref}}, F_{y_{\text{FR}}}^{\text{ref}}\}$.

Sketch of proof: The following proof is an adaptation of the results found in [13] to the specific features of the system at hand. To design the controller and study the closed-loop system, the following candidate Lyapunov function V is considered,

$$V = \frac{1}{2} S^{\text{T}} S. \tag{25}$$

If the sliding surface is attractive for the system, then the front lateral forces will track their reference values. For the sliding surface to be attractive,

$$\dot{S} = 0, \quad \text{that is,} \tag{26}$$

$$C_s \dot{x} = 0. \tag{27}$$

u_{eq} and u_N are generated separately. First, the equivalent control u_{eq} is computed assuming $e = 0$ and $u = u_{\text{eq}}$. Then substituting $\dot{x}$ from Equation (10) in Equation (27) gives

$$C_s (Ax + B_1 u_{\text{eq}} + B_2 r) = 0. \tag{28}$$

After manipulation:

$$u_{\text{eq}} = -(C_s B_1)^{-1} C_s (Ax + B_2 r). \tag{29}$$

$C_s B_1 = -D_i$ and $-D_i$ is invertible as D_i is diagonal with tyre cornering stiffness as diagonal elements. Therefore, u_{eq} can be calculated with Equation (29).

Now $\dot{V}$ can be written as

$$\dot{V} = S^{\text{T}} \frac{\partial S}{\partial x} \dot{x} \tag{30}$$

$$= S^{\text{T}} C_s (Ax + B_1 u + B_e e + B_2 r). \tag{31}$$

Substituting $u = u_{\text{eq}} + u_N$, with u_{eq} from Equation (29) and u_N from Equation (22), in Equation (31), yields the following $\dot{V}$ after manipulation.

$$\dot{V} = -\|{B_1}^{\text{T}} C_s^{\text{T}} C_s x\|_2 (\rho + \alpha) + (C_s x)^{\text{T}} C_s B_e e. \tag{32}$$

Now $B_e = \left[\begin{smallmatrix} B_i & 0 \\ 0 & -D_i \end{smallmatrix}\right]$ is written as

$$B_e = \begin{bmatrix} B_i & 0 \\ 0 & -D_i \end{bmatrix} = \begin{bmatrix} B_i \\ -D_i \end{bmatrix} X. \tag{33}$$

Solving the above matrix equation for X gives

$$X = (B_i{}^{\mathrm{T}} B_i + D_i{}^{\mathrm{T}} D_i)^{-1} [B_i^{\mathrm{T}} B_i \;\; D_i^{\mathrm{T}} D_i]. \tag{34}$$

Now using Equation (33) in Equation (32) gives

$$\begin{aligned} \dot{V} &= -\|B_1{}^{\mathrm{T}} C_s^{\mathrm{T}} C_s x\|_2 (\rho + \alpha) + (C_s x)^{\mathrm{T}} C_s \begin{bmatrix} B_i \\ -D_i \end{bmatrix} X e \\ &= -\|B_1{}^{\mathrm{T}} C_s^{\mathrm{T}} C_s x\|_2 (\rho + \alpha) + (C_s x)^{\mathrm{T}} C_s B_1 X e \\ &= -\|B_1{}^{\mathrm{T}} C_s^{\mathrm{T}} C_s x\|_2 (\rho + \alpha) + (C_s x)^{\mathrm{T}} C_s B_1 (B_i{}^{\mathrm{T}} B_i + D_i{}^{\mathrm{T}} D_i)^{-1} [B_i{}^{\mathrm{T}} B_i \;\; D_i{}^{\mathrm{T}} D_i] e. \end{aligned} \tag{35}$$

Since $\|(B_i^{\mathrm{T}} B_i + D_i^{\mathrm{T}} D_i)^{-1} [B_i^{\mathrm{T}} B_i \;\; D_i^{\mathrm{T}} D_i] e\|_2 < \rho$, the above equation implies that $\dot{V} \leq -\|B_1^{\mathrm{T}} C_s^{\mathrm{T}} C_s x\|_2 \alpha$. As $\alpha > 0$, this proves the negative definiteness of the candidate Lyapunov function V . Therefore, the sliding surface is attractive for the closed-loop system.

Chattering: In order to avoid chattering associated with the SMC, the control input is made continuous if the 2-norm of the sliding surface lies inside a boundary layer of 2ϵ thickness. This is shown in Equation (36).

$$u = \begin{cases} u_{\mathrm{eq}} - \dfrac{B_1 C_s^{\mathrm{T}} C_s x}{\|B_1 C_s^{\mathrm{T}} C_s x\|_2} (\rho + \alpha) & \text{if } \|S\|_2 \geq \epsilon, \\ u_{\mathrm{eq}} + p(x) & \text{otherwise.} \end{cases} \tag{36}$$

Here $p(x)$ is the following function,

$$p(x) = -\frac{B_1 C_s^{\mathrm{T}} C_s x}{\|B_1 C_s^{\mathrm{T}} C_s x\|_2} (\rho + \alpha) \frac{\|S\|_2}{\epsilon}. \tag{37}$$

The control input in Equation (36) attracts the vehicle states to the boundary layer. If the vehicle is within the boundary layer, then it provides a continuous control input that approximates the otherwise discontinuous control input so that chattering is avoided.

3.1.3. *TUCC tuning*

The TUCC has three tuning parameters, ϵ, α and ρ. As the sum of α and ρ is used to calculate the control input, tuning one of them is enough. Therefore, α is set to 0.006 and ρ is tuned. The value of ϵ determines how much chattering is observed in the control input u. For tuning ϵ, a steady-state cornering with RoC 152.4 m and $v = 80$ km/h is simulated with the TUCC ON. The value of ϵ, by influencing the transition from the continuous operation mode to the effective sliding mode, affects the stability. If ϵ is too small, the transition between the two operating modes causes sustained oscillations. It should be noted that for non-zero ϵ values, once the vehicle states are inside the boundary layer, until the vehicle states go outside the boundary layer, the control input is a continuous approximation of the discontinuous control as shown in Equations (36) and (37).

The value of ρ is tuned using a sine with dwell (SWD) manoeuvre. In a SWD manoeuvre, the vehicle goes at a constant speed of 80 km/h and the driver steering wheel input is a SWD

signal. The top plot in Figure 7 shows the SWD steering profile. The SWD manoeuvre has a frequency of 0.7 Hz without the 0.5 s pause during the second peak. The SWD manoeuvre is chosen as it is known to excite the vehicle's nonlinearities.

The value of ρ is first set to its lower limit calculated with the help of Equations (10) and (33) during a SWD manoeuvre with amplitude 150°. Further it is increased. For higher values, higher overshoots are observed in the yaw rate and lateral acceleration once the SWD cycle is over. ρ is increased till 0.104 where the overshoot is less than 10%. Finally, the tuned value of 0.104 is multiplied by the road–tyre friction μ so that the steering actuation is scaled depending on the friction.

3.1.4. *Gain scheduling to improve robustness to vehicle speed*

The TUCC has been derived for the 80 km/h case. Therefore, when the vehicle speed is varied, the upper bound of lumped vector norm $\|(B_i^{\mathrm{T}}B_i + D_i^{\mathrm{T}}D_i)^{-1}[B_i^{\mathrm{T}}B_i \;\; D_i^{\mathrm{T}}D_i]e\|_2$, that is, ρ might be different. As a consequence, if simulations are run at different speeds with the same TUCC, there may be a loss of performance. This can be avoided by gain scheduling with the vehicle speed. This way the value of ρ will be more accurate. Therefore, a speed-dependent gain scheduling is developed so that the TUCC is robust to vehicle speed. The changes in the TUCC are the vehicle model used for SMC design and the SMC parameter ρ. The vehicle model is linearised at different speeds so that the model's speed dependency is considered. ρ is tuned in closed loop with the TUCCs designed at different vehicle speeds. The gain scheduling uses convex summation of control inputs calculated at two different vehicle speeds. The following equations explain the convex summation used.

$$u_{\mathrm{convex}} = G_{v_1}u_{v_1} + G_{v_2}u_{v_2} \quad \text{where} \tag{38}$$

$$G_{v_1} = \frac{v - v_1}{10}, \tag{39}$$

$$G_{v_2} = 1 - G_{v_1}, \tag{40}$$

$$v_2 - v_1 = 10, \tag{41}$$

$$v_1 < v \leq v_2. \tag{42}$$

Here u_{convex} is the control input calculated using convex summation, G_{v_1} and G_{v_2} are non-negative real numbers, u_{v_1} and u_{v_1} are the TUCC control inputs calculated at vehicle speeds v_1 and v_2, respectively, and v is the vehicle speed. The convex summation is done using different control inputs and not using convex summation of system matrices as the latter will require real-time controller design which is computationally expensive. Outside the speed range $(v_1, v_2]$, gain scheduling continues in the same way.

4. Results

Both the TUCC as well as SACs are implemented in Simulink environment and co-simulated with CarSim, a multi-body vehicle simulator. Several simulation experiments are performed to study the closed-loop performance. First the vehicle is simulated for a ramp steering input. Here the objective is to study whether the TUCC is able to meet its objective in Equation (12). Next, lateral stability is studied with a SWD manoeuvre. Then, vehicle lateral acceleration is studied for higher steering wheel angles. Finally, the controller is tested for its robustness to vehicle speed, force measurement noise and road–tyre friction.

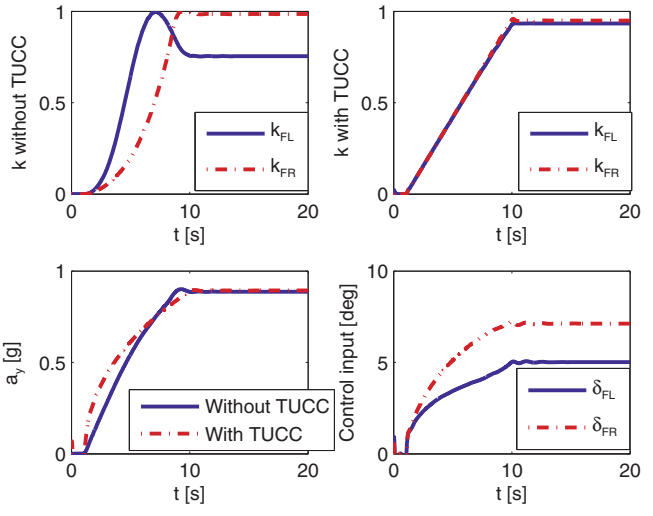

Figure 6. Simulation results for a ramp input with and without TUCC.

First the ramp steering input case is discussed. In this simulation experiment, the vehicle goes at a constant speed of 80 km/h and the steering wheel input from the driver is increased from 0° to 150° in 0–10 s. After $t = 10$ s, the steering wheel input is kept constant at 150°.

The vehicle is simulated for this driver input with and without the TUCC. Further, it is studied whether the TUCC objective in Equation (12) is met. From Figure 6, the following observations can be made.

- Without TUCC, the TUCs of the front tyres are not equal whereas with TUCC, the tyres are equally utilised, that is, $k_{FL} = k_{FR}$.
- With TUCC, the lateral acceleration a_y has less overshoot when the ramp reaches its maximum value at $t = 10$ s.
- It should be noted that there is not much improvement in the closed-loop lateral acceleration because the steering wheel angle (150°) is not considerably higher than the 135° threshold shown in Figure 5. Such a case where the steering wheel angle is considerably higher than the 135° threshold is discussed in Section 4.3.

Now that the controller is found to be able to meet its objective, in a quasi-static test, its dynamical properties are further studied.

4.1. *Lateral dynamics stability*

The top plot in Figure 7 shows the applied SWD steering input to study lateral dynamics stability. The SWD manoeuvre is known to excite the vehicle's nonlinearities as the tyre forces could reach their nonlinear operating region depending on the vehicle speed. Whether the vehicle is stable or unstable is defined using the stability criteria (SC) in Equations (43) and (44).[21]

$$\mathrm{SC}_1 = \frac{\dot{\psi}_{t_0+1.00}}{\dot{\psi}_{\mathrm{Peak}}} \times 100 \leq 35\%, \tag{43}$$

$$\mathrm{SC}_2 = \frac{\dot{\psi}_{t_0+1.75}}{\dot{\psi}_{\mathrm{Peak}}} \times 100 \leq 20\%. \tag{44}$$

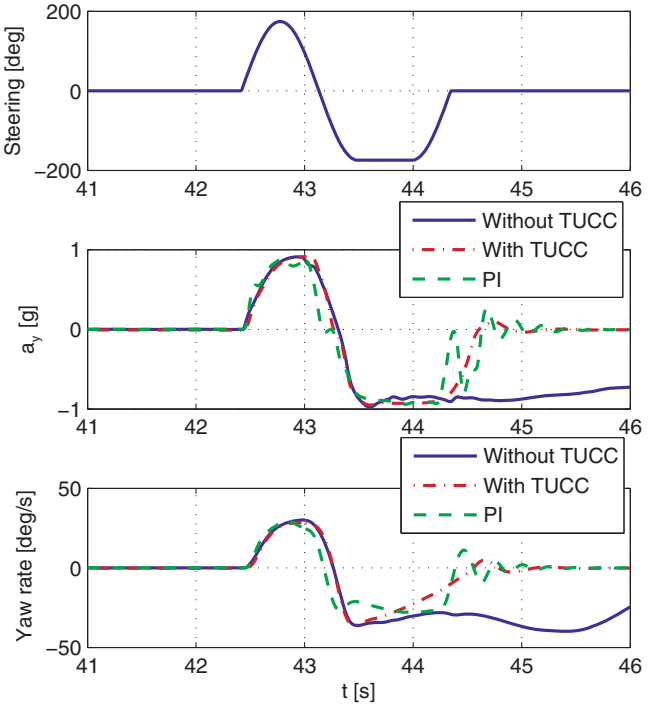

Figure 7. Simulation results for SWD manoeuvre with and without TUCC.

Here, SC_1 means that, after 1.0 s of the SWD steering cycle, the yaw rate of the vehicle has to be less than or equal to 35% of the first local peak yaw rate produced by the steering reversal. SC_2 means that, after 1.75 s of the SWD steering cycle, the yaw rate of the vehicle has to be less than or equal to 20% of the first local peak yaw rate produced by the steering reversal.

In order to compare the proposed controller, a proportional-integral (PI)-based VDC is used. The PI-based VDC controls the vehicle yaw rate using steering actuator and it employs a typical yaw rate reference model.[1] Steering actuator is chosen for the PI-based VDC because the TUCC uses steering actuator and this way, the controllers' performances can be compared for equal control input costs. Therefore, the PI-based VDC is tuned such that the quadratic control input cost is equal to that of the TUCC for the chosen SWD manoeuvre.

In Figure 7, the lateral acceleration and yaw rate during the SWD manoeuvre are also shown. The following observations can be made from these plots.

- Without TUCC, the yaw rate is not coming back to zero once the SWD cycle is over. This implies that the vehicle is spinning out of control. Whereas with TUCC, the yaw rate comes back to zero once the SWD cycle is over.
- SC_1 and SC_2 are calculated from the yaw rate plots and are given in Table 1. It is clear that without TUCC, both the SC in Equations (43) and (44) are not met whereas with TUCC, they are met.
- The TUCC is able to maintain lateral acceleration a_y as defined in Equation (15), especially once the SWD cycle is over, that is, it is able to bring a_y to zero. Whereas without the TUCC, a_y does not come back to zero and this means the vehicle is oversteering, a behaviour the driver is not desiring with his steering input.

Table 1. SC_1 and SC_2 for SWD manoeuvre with and without the TUCC.

TUCC status	SC_1	SC_2	$SC_1 \leq 35\%$	$SC_2 \leq 20\%$
OFF	109.52	66.21	No	No
ON	− 0.86	0.47	Yes	Yes

- The PI-based VDC is able to stabilise the vehicle. However, the yaw rate has an overshoot of the order 11° /s once the SWD is over. Whereas for the same quadratic control input cost, that is, for the same control effort, the TUCC stabilises the vehicle without such high overshoot in the yaw rate.

These considerations show that the TUCC is able to keep the vehicle stable for the applied SWD steering input whereas without the TUCC, the vehicle is not stable.

In the top left and right plots of Figure 8, the TUCs are shown for the SWD manoeuvre. The following observations can be made from the TUC plots.

- With control, the front TUCs are closer to being equal when compared with the case without control, especially during the second half cycle of the SWD.
- Without control, the TUCs are not brought close to zero after the SWD cycle and this corresponds to the vehicle spinning out of control. Whereas with control, the TUCs are brought close to zero once the SWD cycle is over, which means the vehicle is not spinning out of control, hence it is stable.

In conclusion, the application of the SWD manoeuvre has shown that using the TUCC with the objective of keeping the front left and right TUCs equal can keep the vehicle stable in situations where the vehicle would have lost stability. In the bottom left and right plots of Figure 8, break up of the SMC inputs generated by the TUCC, u_{eq} and u_N, is shown. In Figure 9, the control inputs generated by both controllers are shown.

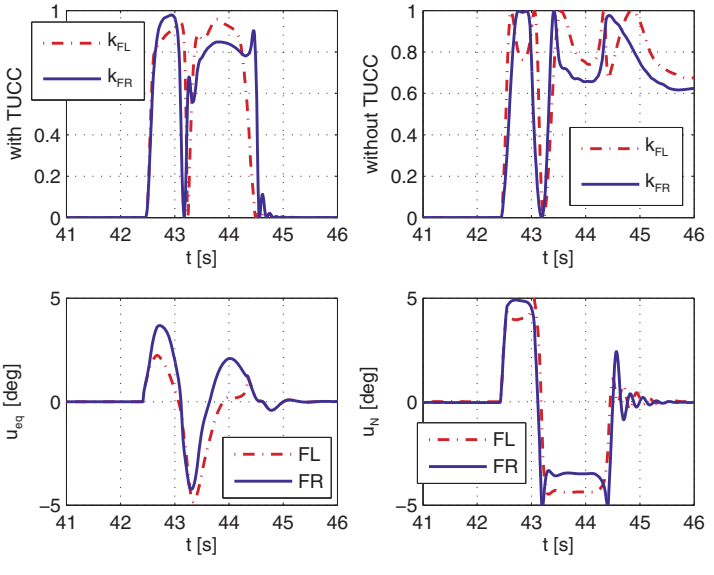

Figure 8. TUCs and control inputs $\{u_{\text{eq}}, u_N\}$ during the SWD manoeuvre.

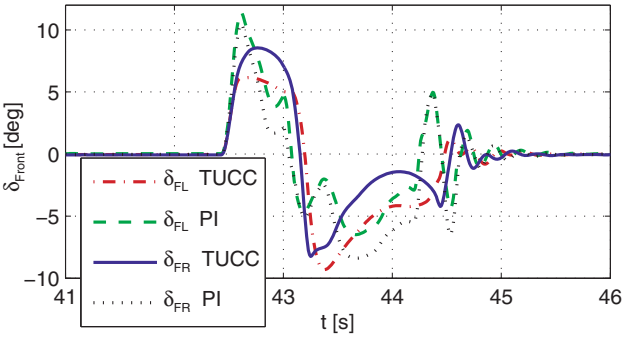

Figure 9. Control inputs generated by the TUCC and PI-based VDC.

4.2. *Robustness to SWD amplitude*

For SWD amplitudes higher than the one in Figure 7, it is observed that the vehicle states, vehicle side slip angle and yaw rate, and the outputs, front left and right lateral tyre forces, are almost equal to the results shown in Section 4.1. This is because the force references in Equations (18) and (19) have limits as they are calculated based on the bounded lateral acceleration reference in Equation (15).

4.3. *Maintaining the maximum possible lateral acceleration for higher steering angles*

In this section, the vehicle lateral acceleration is studied for increasing steering wheel angle at a constant speed of 80 km/h. The steering wheel angle profile is shown in the bottom right plot of Figure 10.

Further, the vehicle lateral acceleration is studied with and without the TUCC. From Figure 10, it can be observed that without TUCC, the lateral acceleration reduces as the

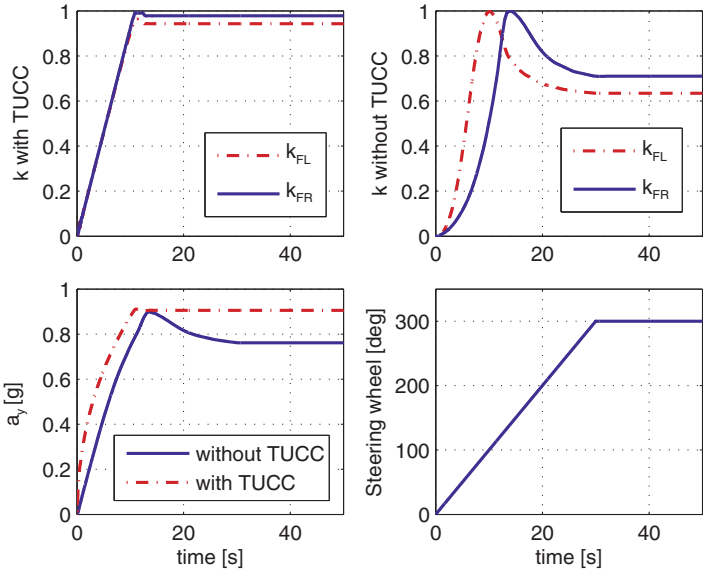

Figure 10. Effect of the TUCC on lateral acceleration for higher steering wheel angles.

steering wheel angle is increased to more than 135°. Whereas with TUCC, when the steering wheel angle is increased to more than 135°, the lateral acceleration is maintained very close to its maximum possible value. Without TUCC, it can be observed that the TUCs reduce for steering wheel angles higher than 135° whereas with TUCC, the TUCs are maintained very close to 1, hence the lateral acceleration is maintained close to its maximum possible value. Such a situation can happen when an average skilled driver applies steering higher than a certain threshold assuming that he will get more lateral acceleration. It must be noted that this benefit is applicable only on road conditions that facilitates a peak followed by negative slope in lateral tyre force characteristics.

4.4. *Robustness to vehicle speed*

In this section, the speed-dependent gain scheduled controller is compared against the non-scheduled controller. As shown in Figure 11(a), with the initial TUCC, that is, the one designed with the model linearised at 80 km/h, as the vehicle speed is increased from 80 to 100 km/h, the vehicle is not following its lateral acceleration reference and the SC in Equation (43) is not met. But with the gain scheduled controller, the vehicle is no more unstable, whereas the open-loop case is unstable. The speed-dependent gain scheduling increases the controller robustness.

Figure 11(b) shows the case when the vehicle speed is increased to 120 km/h. With the gain scheduled controller, the vehicle is observed to be stable, whereas in the open-loop case the vehicle is spinning out of control. However, the closed-loop performances are not as good as compared to slower vehicle speeds.

4.5. *Robustness to measurement noise*

In this section, simulation experiments are performed to study the closed-loop robustness to measurement noise of the force sensors. The lateral and vertical tyre force measurements from CarSim is polluted with a uniform distributed noise in the range [−500 N, 500 N]. This is approximately 10% of the force range. Figure 12 shows a sample longitudinal force measurement from our test vehicle. It is clear from the sample measurement that the peak-to-peak noise is less than the considered range [−500 N, 500 N]. Yaw rate measurement is also polluted with a uniform distributed noise in the range [−2.5°/s, 2.5°/s] which is approximately 10% of the yaw rate seen during the SWD simulation.

Figure 13(a) shows the lateral acceleration and yaw rate from this study. The simulations are done at a vehicle speed of 80 km/h. Both TUCC and PI-based VDC have the same tuning settings as in Section 4.1. It is clear from these plots that the TUCC is able to keep the vehicle stable when compared with the uncontrolled case and there is not much difference with respect to the noiseless case. It is also observed that the PI-based VDC is able to stabilise the vehicle in the presence of measurement noise.

In Figure 13(b), the lateral tyre forces of the front tyres and the control inputs generated by the controllers are plotted. It can be observed from the lateral force plots that although the noise level is quite prominent, the control inputs shown in the bottom plot are able to keep the vehicle stable.

4.6. *Robustness to road–tyre friction*

In this section, simulation experiments are performed to study the closed-loop robustness to different peak road–tyre friction. The simulations are done at 80 km/h using SWD steering

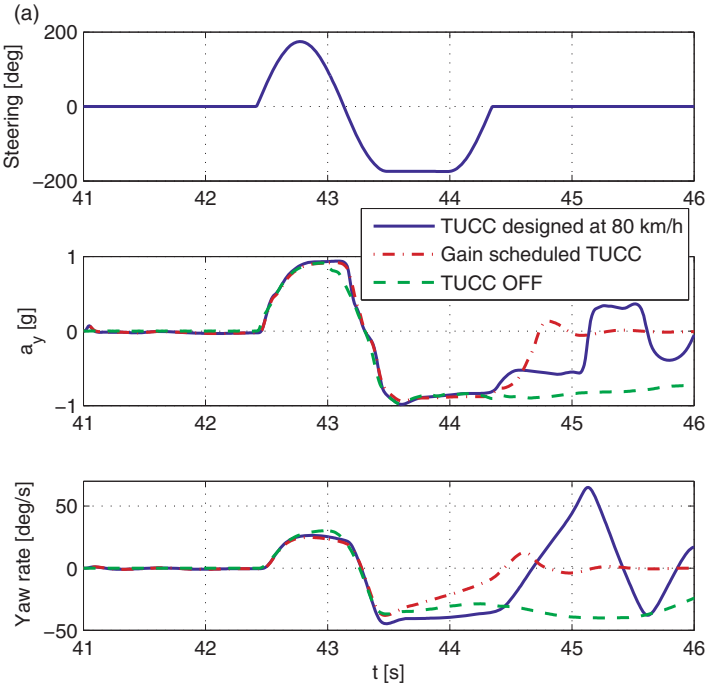

At vehicle speed 100 km/h.

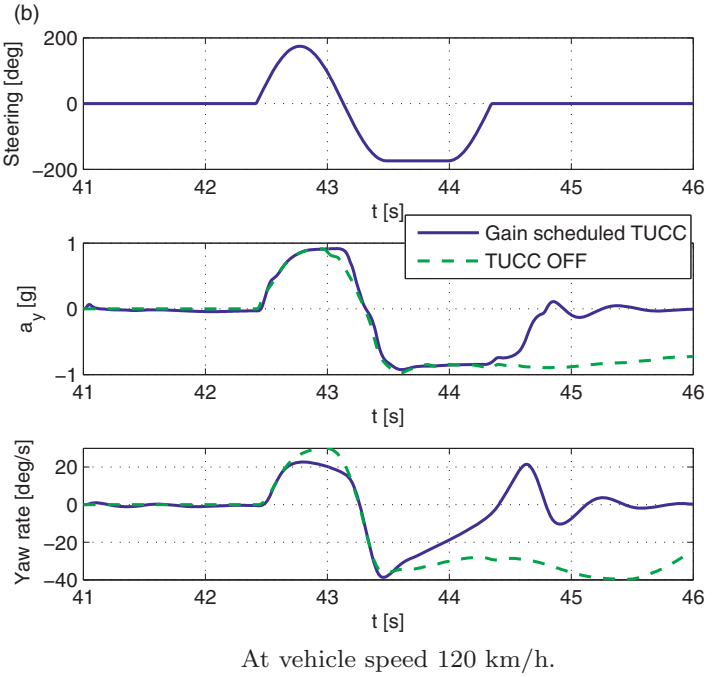

At vehicle speed 120 km/h.

Figure 11. Simulation results for SWD manoeuvre with speed-dependent gain scheduled controller.

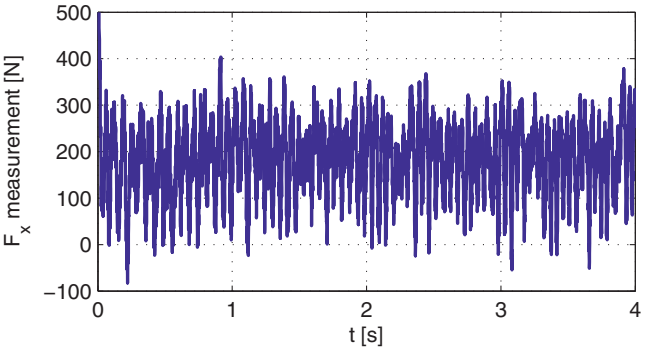

Figure 12. A sample longitudinal force measurement from the test vehicle fitted with the tyre force sensors.

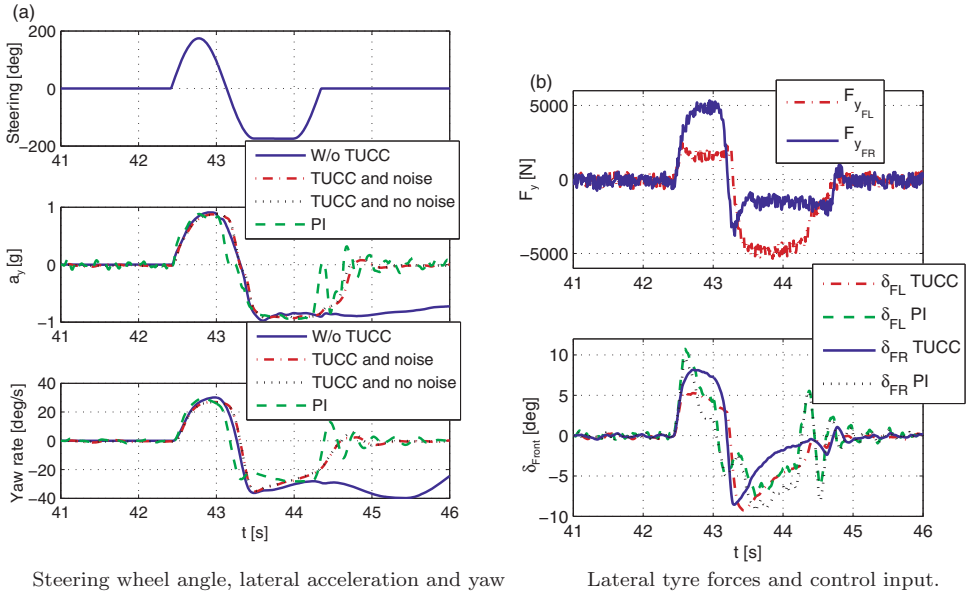

Steering wheel angle, lateral acceleration and yaw rate.

Lateral tyre forces and control input.

Figure 13. Simulation results for SWD manoeuvre with force measurement noise.

input and the results are shown in Figure 14. In these simulations, both TUCC and PI-based VDC have the same tuning settings as in Section 4.1. Figure 14(a) shows the simulation results with peak road–tyre friction 0.6. The following observations can be made.

- Without TUCC, the vehicle yaw rate and lateral acceleration do not return to zero once the SWD cycle is over. Instead there is a very high overshoot. With TUCC, they return to zero.
- With the PI-based VDC, the yaw rate returns to zero; however, there is a considerable lag, that is, the yaw rate returns to zero approximately 1 s after the SWD ends. Therefore, the TUCC performance is better than the PI-based VDC.

Figure 14(b) shows the simulation results with peak road–tyre friction 0.3. The following observations can be made.

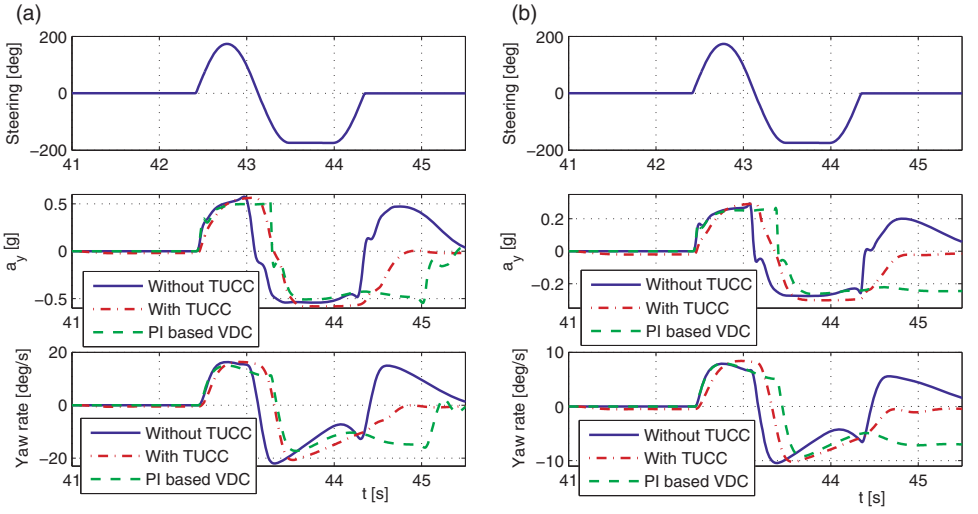

With peak road-tyre friction 0.6. With peak road-tyre friction 0.3.

Figure 14. Simulation results for SWD manoeuvre with different peak road–tyre friction values.

- Without TUCC, the vehicle yaw rate and lateral acceleration do not return to zero once the SWD cycle is over. This implies that the vehicle is spinning undesirably. With TUCC, the vehicle is stable.
- The PI-based VDC is not able to stabilise the vehicle.

Therefore, it is seen that the TUCC is robust to road–tyre friction. The main reason for the robustness is that the TUCC controls the tyre utilisation coefficients which depend on the tyre forces and road–tyre friction, and the tuning parameter ρ depends on the friction.

5. Conclusions

A new method for lateral vehicle dynamics control using tyre force measurements and active front steering is proposed. First, a simulation study exemplifies the fact that during cornering, the TUCs are not evenly employed. This can get one of the front tyres to hit saturation before the others, thereby possibly causing discomfort for an average driver or even an unstable situation. Next, the TUCC is proposed to address this issue with the objective of keeping the front left and front right TUCs equal, that is, $k_{\mathrm{FL}} = k_{\mathrm{FR}}$. As a consequence of the proposed TUCC, the vehicle is able to maintain the maximum possible lateral acceleration when a driver applies higher steering angles. The TUCC is designed using the SMC method. The proposed controller is tested in several conditions ranging from quasi-steady state cornering to a more dynamically demanding SWD manoeuvre. During the ramp steering cornering, the TUCC is observed to be able to achieve the control objective $k_{\mathrm{FL}} = k_{\mathrm{FR}}$. During the SWD manoeuvre, it is observed that the vehicle is stable with the TUCC, whereas the car goes unstable without the TUCC.

Second, another simulation study exemplifies that when an average driver applies steering higher than a certain threshold, assuming that he will get more lateral acceleration, he might in fact be settling for a lesser lateral acceleration. Whereas with the TUCC, lateral acceleration is maintained very close to its maximum in such driving situations, thereby assisting the driver.

The TUCC is also found to be robust for different SWD amplitudes. In order to make the TUCC robust for different vehicle speeds, a speed-dependent gain scheduling is used. The closed-loop system is further tested in the presence of measurement noise and is found to be robust. Finally, the controller is studied for various peak road–tyre friction values and is found to be robust.

This work has demonstrated tyre force-based lateral vehicle dynamics control in simulation environment. At present, vehicle side slip angle estimation using tyre force measurements is being studied. In addition, the road–tyre friction estimator proposed in [16] is being developed and studied as friction estimation is needed to implement the proposed controller. Future works aim at testing the proposed control scheme on an instrumented vehicle. The next step will also involve studying the use of other actuators, starting with braking actuators.

Disclosure statement

No potential conflict of interest was reported by the authors.

Note

1. The extreme case is represented by a vehicle that is already accelerating at the limit of the longitudinal force ($F_x = F_{x_{\max}}$). If a steering input that translates into a desired k_F^{req}, according to Equation (16), is given in this condition, the lateral force reference generation in Equations (18)–(19) would yield 0 and the vehicle would not steer. This could be arguable as the vehicle would not be able to steer and avoid an obstacle; but note that this is a limitation of the actuation (we are assuming to only have automatic control of steering) and not of the control algorithm. It is in fact preferable not to steer and let the driver reduce the throttle rather than letting the driver steer but completely lose control of the vehicle. For more details on how to address the above issue if active braking is available, see [10].

References

[1] Doumiati M, Sename O, Martinez J, Dugard L. Vehicle yaw control via coordinated use of steering/braking systems. IFAC World Congress; 2011; Milan, Italy.

[2] Shim T, Margolis D. Using μ feedforward for vehicle stability enhancement. Vehicle Sys Dyn. 2001;35(2):103–119.

[3] Madhusudhanan AK, Corno M, Bonsen B, Holweg E. Solving algebraic Riccati equation real time for integrated vehicle dynamics control. American Control Conference, 2012 June 27–29; Montreal, Canada; p. 3593–3598.

[4] Buckholtz KR. Use of fuzzy logic in wheel slip assignment – part I: yaw rate control. SAE 2002 World Congress, Detroit, MI; 2002.

[5] Bakker E, Nyborg L, Pacejka HB. Tyre modeling for use in vehicle dynamics studies. SAE Technical Paper No. 870421.

[6] Braghin F, Brusarosco M, Cheli F, Cigada A, Manzoni S, Mancosu F. Measurement of contact forces and patch features by means of accelerometers fixed inside the tire to improve future car active control. Vehicle Sys Dyn. 2006;44(suppl.1):3–13. doi:10.1080/00423110600867101.

[7] Van Leeuwen BG, Holweg EGM, Wit F, Zaaijer E, Ballegooij S. Measurement device for measuring radial and/or axial forces. U.S. Patent No. 6,920,801. Washington, DC: U.S. Patent and Trademark Office; 2005.

[8] Corno M, Gerard M, Verhaegen M, Holweg E. Hybrid ABS control using force measurement. IEEE Trans Control Syst Technol. 2012;20(5):1223–1235.

[9] de Bruijn E, Gerard M, Corno M, Verhaegen M, Holweg E. On the performance increase of wheel deceleration control through force sensing. IEEE International Conference on Control Applications; 2010; Yokohama, Japan; p. 161–166.

[10] Gerard M, Corno M, Verhaegen M, Holweg E. Force-based ABS control using lateral force measurement. ASME 2011 Dynamic Systems and Control Conference and Bath/ASME Symposium on Fluid Power and Motion Control (DSCC2011), Vol. 2; 2011; Arlington, VA; p. 831–837.

[11] Madhusudhanan AK, Corno M, Holweg E. Lateral vehicle dynamics control based on tyre utilization coefficients and tyre force measurements. 52nd IEEE Conference on Decision and Control; 2013 December 10–13; Florence, Italy; p. 2816–2821.

[12] CarSim Math Models. Mechanical Simulation Corporation Brochures & Tech Memos; 2012.

[13] DeCarlo RA, Zak SH, Matthews GP. Variable structure control of nonlinear multivariable systems: a tutorial. Proc IEEE. 1988;76(3):212–232.
[14] Tongue B. Two brains, one car – actively controlled steering. IEEE Control Syst. 2005;25(5):14–17.
[15] Yih P, Gerdes JC. Modification of vehicle handling characteristics via steer-by-wire. IEEE Trans Control Syst Technol. 2005;13(6):965–976.
[16] Rajamani R, Phanomchoeng G, Piyabongkarn D, Lew JY. Algorithms for real-time estimation of individual wheel tire-road friction coefficients. IEEE/ASME Trans Mech. 2012;17(6):1183–1195.
[17] Villagra J, d'Andréa-Novel B, Fliess M, Mounier H. A diagnosis-based approach for tire-road forces and maximum friction estimation. Control Eng Pract. 2011;19(2):174–184.
[18] Ghandour R, Victorino A, Doumiati M, Charara A. Tire/road friction coefficient estimation applied to road safety, 18th Mediterranean Conference on Control & Automation (MED); 2010 June 23–25; Marrakech, Morocco; p. 1485–1490.
[19] Hartweg CP. Fahrzeugstabilisierung durch reifenmodellbasierte Schätzung des Kraftschlusspotentials. FKA; 2011; Aachen, Germany.
[20] Edwards C, Spurgeon SH. Robust output tracking using a sliding-mode controller/observer scheme. Int J Control. 2007;64(5):967–983.
[21] Federal motor vehicle safety standards (FMVSS) No. 126 – electronic stability control systems. National Highway Traffic Safety Administration, U.S. Department of Transportation; 2007; Washington, DC.